Electrically-tuneable non-equilibrium optical response of graphene

Eva A. A. Pogna[1,2], Andrea Tomadin[3], Osman Balci[4], Giancarlo Soavi[4,5,6], Ioannis Paradisanos[4], Michele Guizzardi[1], Paolo Pedrinazzi[7], Sandro Mignuzzi[4], Klaas-Jan Tielrooij[8], Marco Polini[3], Andrea C. Ferrari[4], Giulio Cerullo[1,9]

[1] *Dipartimento di Fisica, Politecnico di Milano, P.zza Leonardo da Vinci 32, Milano 20133, Italy*
[2] *NEST, Istituto Nanoscienze-CNR and Scuola Normale Superiore, P.zza S. Silvestro 12, Pisa 56127, Italy*
[3] *Dipartimento di Fisica, Università di Pisa, Largo Bruno Pontecorvo 3, Pisa 56127, Italy*
[4] *Cambridge Graphene Centre, University of Cambridge, 9 JJ Thomson Avenue, Cambridge CB3 0FA, UK*
[5] *Institute of Solid State Physics, Friedrich Schiller University Jena, Jena 07743, Germany*
[6] *Abbe Center of Photonics, Friedrich Schiller University Jena, Jena 07745, Germany*
[7] *L-NESS, Department of Physics, Politecnico di Milano, Via Anzani 42, Como 22100, Italy*
[8] *Catalan Institute of Nanoscience and Nanotechnology (ICN2), BIST & CSIC, Campus UAB, Bellaterra (Barcelona) 08193, Spain*
[9] *Istituto di Fotonica e Nanotecnologie, Consiglio Nazionale delle Ricerche, P.zza L. da Vinci 32, Milano 20133, Italy*

The ability to tune the optical response of a material *via* electrostatic gating is crucial for optoelectronic applications, such as electro-optic modulators, saturable absorbers, optical limiters, photodetectors and transparent electrodes. The band structure of single layer graphene (SLG), with zero-gap, linearly dispersive conduction and valence bands, enables an easy control of the Fermi energy E_F and of the threshold for interband optical absorption. Here, we report the tunability of the SLG non-equilibrium optical response in the near-infrared (1000-1700nm/0.729-1.240eV), exploring a range of E_F from -650 to 250 meV by ionic liquid gating. As E_F increases from the Dirac point to the threshold for Pauli blocking of interband absorption, we observe a slow-down of the photobleaching relaxation dynamics, which we attribute to the quenching of optical phonon emission from photoexcited charge carriers. For E_F exceeding the Pauli blocking threshold, photobleaching eventually turns into photoinduced absorption, due to hot electrons' excitation increasing SLG absorption. The ability to control both recovery time and sign of non-equilibrium optical response by electrostatic gating makes SLG ideal for tunable saturable absorbers with controlled dynamics.

Single layer graphene (SLG) has unique optoelectronic and photonic properties[1–3], which stem from the physics of its massless Dirac fermions. These include high electron mobility (>100,000 $cm^2V^{-1}s^{-1}$ at room temperature (RT)[4–7]), broadband optical absorption[8], tunability of the Fermi energy E_F *via* electrostatic gating[9] resulting from the linear dispersion of its conduction (CB) and valence bands (VB), and a vanishing density of electronic states at the Dirac point[10].

Light absorption in SLG is due to the interplay of intraband[11–13] and interband[16, 17] transitions. In undoped graphene, the first ones dominate in the THz[14] and microwaves[15] ranges, and the second ones[16] in the near-infrared (NIR)[17] and visible (VIS)[16] ranges. Electrical control of E_F, by exploiting the band-filling effect[18], allows one to vary the density of electronic states available for both intraband[17] and interband transitions[3, 18], thus affecting the linear absorption of SLG over a broad range from THz[19–23] to NIR[24–27] and VIS[28]. This has led to the development of SLG-based electro-optic modulators[3, 24, 25, 27, 29–33], which can reach higher modulation speed (up to 200GHz[34]) than $LiNbO_3$[35] and Si[36] devices, due to the superior mobility of SLG charge carriers, and have demonstrated high modulation depths both in amplitude (up to$\sim$ 60%)[3, 19, 21, 24, 26] and phase (up to$\sim 65°$)[3, 31] .

SLG also exhibits large nonlinear optical response[37, 40–42, 48], due to a strong coupling to light. The third-order nonlinear optical susceptibility of SLG in the NIR at 0.7eV is $\chi^3 \sim 5\times10^{-18}$ m^2V^{-2}[37], several orders of magnitude higher than in dielectrics (*e.g.* $\chi^3 \sim 10^{-22}$ m^2V^{-2} for SiO_2[38]) and atomically thin semiconductors (*e.g.* $\chi^3 \sim 6\times10^{-20}$ m^2V^{-2} for single layer WSe_2[39]). Nonlinearities of order higher than the third have been exploited for high-harmonics generation in SLG[40, 41]. The strong nonlinear response results also in saturable absorption[43], optical Kerr effect[44], and optical bistability[45, 46], *i.e.* the ability to provide two stable optical outputs for a specific light input[47]. Doping control *via* external gating allows one to tune also the nonlinear optical response of SLG, resulting in gate-tunable third-harmonic generation[37, 42, 48] and four-wave-mixing[49].

The doping dependence of the transient absorption properties of SLG when brought out of equilibrium remains still largely unexplored, with studies limited to the THz range[50–52], discussing the tuning of intraband photoconductivity with doping[50–52]. The modulation of interband absorption in NIR and VIS is more challenging to study, due to the need of $E_F \sim$0.5eV in order to cross the Pauli blocking threshold, above which the non-equilibrium optical properties have been only theoretically explored[53].

The non-equilibrium optical response of SLG is crucial for optoelectronic applications, such as

photodetectors[54], relying on the relaxation dynamics of photoexcited charge carriers. Numerous ultrafast optical spectroscopy experiments have been performed on SLG[55–59] to investigate the charge-carriers relaxation dynamics by looking at the modifications it induces on the SLG absorption properties. In a pump-probe experiment, the system is photoexcited by an optical pulse, the pump, whose duration is to be shorter than the timescale of the relaxation processes under investigation. The relaxation of the photoexcited system is then monitored by detecting the absorption of a second optical pulse, the probe, as function of the time delay with respect to the pump pulse[60].

In SLG, interband absorption of the pump pulse induces out-of-equilibrium distributions of holes (h) and electrons (e) in VB and CB, respectively, peaked at $\pm\hbar\omega_{pump}/2$, where $\hbar\omega_{pump}$ is the pump photon energy. Carrier-carrier scattering drives the ultrafast e-h thermalization on a time-scale $\tau_{th} < 20$fs[59] from out of equilibrium, to an hot Fermi-Dirac distributions (HFD) with defined electronic temperature T_e. The HFD can be detected in a pump-probe experiment as a photobleaching (PB) signal[55–57], *i.e.* decreased probe absorption compared to equilibrium, due to Pauli blocking of interband transitions caused by the photo-generated e/h. The excess energy of the hot charge-carriers is released to the lattice *via* electron-phonon scattering with optical phonons[61, 62], which in turn are anharmonically coupled to acoustic phonons[61–63]. Hot carriers cooling occurs on a few-ps time-scale[55–57, 59, 63] and is influenced, through the activation of additional relaxation channels, by the dielectric environment (*e.g. via* near-field coupling to hyperbolic optical phonons of the substrate or encapsulant material[64]). Defects can also accelerate the cooling *via* electron-phonon interaction by acting as scattering centres mediating the direct coupling of hot charge carriers with finite momentum acoustic phonons[65–67]. This process, referred to as supercollision[65–67], accelerates the cooling for increasing defect density[68].

Here we investigate the doping dependence of the non-equilibrium optical response of SLG in the NIR range between 0.729 and 1.240eV (1000-1700nm), exploiting ionic liquid gating to tune E_F from -800 to 250meV, thus exceeding the Pauli blocking threshold for interband absorption, achieved when $|E_F| = \hbar\omega_{probe}/2$, where $\hbar\omega_{probe}$ is the photon energy of the probe beam. Applying ultrafast pump-probe spectroscopy with 100fs time resolution, we detect the changes with E_F of amplitude and sign of the differential transmission ($\Delta T/T$), as well as of its relaxation dynamics. Starting from not intentionally doped SLG and increasing E_F, we first observe a rise in the PB amplitude ($\Delta T/T > 0$), in agreement with Ref.[69], together with a slow-down of the PB relaxation dynamics. Above the threshold of Pauli blocking, photoexcitation has an opposite effect on SLG, causing the activation of new absorption channels, as shown by the appearance of a photoinduced absorption (PA) signal ($\Delta T/T < 0$). The $\Delta T/T$ changes are assigned to the doping dependence of the hot carriers cooling dynamics, simulated considering relaxation through emission of optical phonons. The gate tunability of the non-equilibrium optical response paves the way for novel optoelectronic applications, such as saturable absorbers (SA) with gate-tunable response.

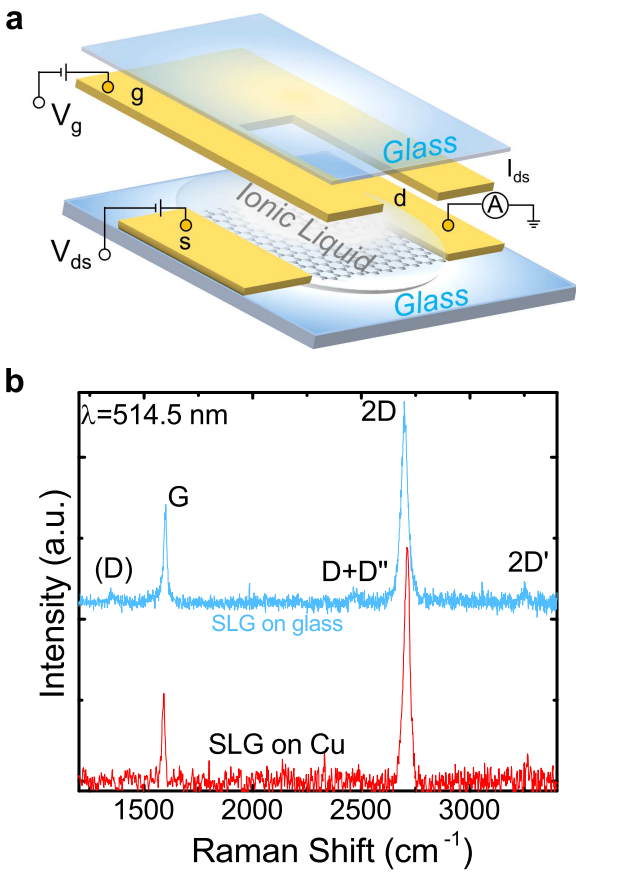

FIG. 1: (**a**) Schematic of device with source (s), drain (d) and gate (g) contacts used to tune the SLG E_F while measuring its transmission properties; (**b**) 514.5 nm Raman spectrum of SLG as-grown and transferred on glass.

RESULTS AND DISCUSSION

We modulate E_F in SLG by means of the electrostatic field effect[70] using an ionic-liquid top-gated field effect transistor (FET) sketched in Fig.1a. The top-gate geometry, with Diethylmethyl (2-methoxyethyl) ammoniumbis - (triflouromethylsulfonyl) imide ($C_6H_{20}F_6N_2O_5S_2$) as ionic liquid, is chosen to allow light measurements in transmission through an$\sim$1cm^2 optical window. The large area (8mm$\times$8mm) SLG is prepared by chemical vapor deposition (CVD) as for Ref.[71]. The device fabrication follows Ref.[72].

Both as grown and transferred SLG are characterized with a Renishaw InVia Raman spectrometer using a 50x objective at 514.5nm, with power on the sample<0.5mW to exclude heating effects. The Raman peaks are fitted with Lorentzians, with error bars derived from the standard deviation across 6 spectra and the spectrometer resolution$\sim$1cm^{-1}. The Raman spectrum of as-grown SLG on Cu is in Fig.1b, after Cu photoluminescence removal[73]. The 2D peak is a single Lorentzian with full-width half maximum FWHM(2D)$\sim$31$\pm$3cm^{-1}, signature of SLG[74]. The G peak position Pos(G) is$\sim$1586$\pm$2cm^{-1}, with FWHM(G)$\sim$16$\pm$3cm^{-1}. The 2D peak position, Pos(2D), is$\sim$2704$\pm$4cm^{-1}, while the 2D to G peak intensity and area ratios, I(2D)/I(G) and A(2D)/A(G), are 3.1$\pm$0.4 and 6.2$\pm$0.7. No D peak is observed, indicating negligible Raman active defects[75, 76].

The Raman spectrum of SLG transferred on glass is in Fig.1b. The 2D peak retains its single-Lorentzian line shape with FWHM(2D)$\sim$36$\pm$1cm^{-1}. Pos(G)$\sim$1597$\pm$1cm^{-1}, FWHM(G) $\sim$15$\pm$1cm^{-1}, Pos(2D)$\sim$2696$\pm$3cm^{-1}, I(2D)/I(G)$\sim$2$\pm$0.2 and A(2D)/A(G) $\sim$4.9 $\pm$0.3 indicating p-doping with $E_{\rm F}$ $\sim$ -230$\pm$80meV[70, 77]. I(D)/I(G) is$\sim$0.06$\pm$0.05, corresponding to a defect density$\sim$2.6$\pm$1.9$\times$10^{10}cm^{-2}[78] for excitation energy 2.41eV and $E_{\rm F}$= -230$\pm$80meV. Pos(G) and Pos(2D) are affected by the presence of strain[79]. For uniaxial(biaxial) strain, Pos(G) shifts by ΔPos(G)/$\Delta\varepsilon$ $\sim$23(60)cm^{-1}\%$^{-1}$[79, 80]. Pos(G) also depends on $E_{\rm F}$[9, 70]. The average doping as derived from A(2D)/A(G), FWHM(G) and I(2D)/I(G), should correspond to Pos(G)$\sim$1588$\pm$1cm^{-1} for unstrained graphene[9, 70]. However, in our experiment Pos(G)$\sim$1597$\pm$1cm^{-1}, which implies a contribution from uniaxial (biaxial) strain$\sim$0.16$\pm$0.02% (0.4$\pm$0.04%)[79, 80].

The gate voltage $V_{\rm g}$ polarizes the ionic liquid leading to the formation of electrical double layers (EDLs), near the SLG and Au interfaces[70, 81], that modulate the carrier density. Since the EDL thickness is$\sim$1nm for ionic liquids[82, 83], the solid-liquid interfacial electric field and the induced charge densities on the surface reach values as large as$\sim$10-20MVcm^{-1} and 10^{14}cm^{-2}[22, 82] even at moderate $V_{\rm g}$ $\sim$1-2V. The transfer characteristics of our device for source-drain bias $V_{\rm ds}$=100mV is in Fig.2a. This exhibits a typical ambipolar behaviour, as seen by the V-shaped gate dependence of the source-drain current $I_{\rm ds}$. The channel resistance peaks at $V_{\rm CNP}$=0.84V, corresponding to the charge neutrality point (CNP), where the density of states in SLG reaches its minimum[22, 23, 84]. $V_{\rm CNP}$ depends on $E_{\rm F}$, on the gate-metal work function[22], and on the choice of contact materials[85].

In order to determine $E_{\rm F}$ as a function of V_g, we measure the static transmission T in the NIR (500-1500meV) with an Agilent Cary 7000 UV-VIS-MIR spectrometer. Fig.2b plots a selection of transmission spectra for different V_g, compared to that at the CNP, evaluated as follows: $\delta T/T = \frac{T(V_{\rm g})-T(V_{\rm CNP})}{T(V_{\rm CNP})}$. T increases with respect to the CNP, *i.e.* $\delta T/T > 0$, when absorption is inhibited by Pauli blocking, due to e in CB (n-doping) or h in VB (p-doping). In terms of probe photon energy, this corresponds to $\hbar\omega_{probe} < 2|E_{\rm F}|$. We estimate $E_{\rm F}$ considering that $\delta T/T$ halves[72] for $\hbar\omega_{probe} = 2|E_{\rm F}|$ at values indicated by black stars in Fig.2b. For probe photon energies $\hbar\omega_{probe} < 2|E_{\rm F}|$, interband absorption is blocked and the

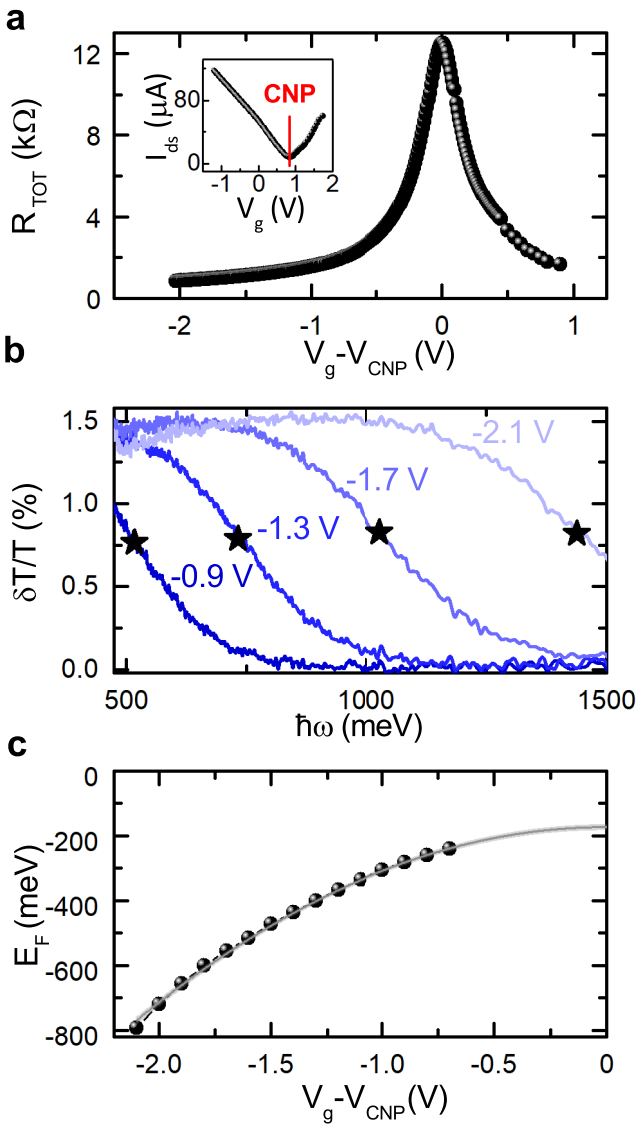

FIG. 2: (**a**) Total resistance $R_{\rm TOT}$ as a function of $V_{\rm g}$-V$_{CNP}$. Inset, drain-source current $I_{\rm ds}$ for $V_{\rm ds}$= 100 mV. (**b**) $\delta T/T$ for different V_g-V$_{CNP}$ (indicated next to the curves) as a function of photon energy $\hbar\omega$ showing the gate tunability of the absorption edge for interband transitions; (**c**) $E_{\rm F}$ determined from $\delta T/T$ as a function of V_g-V$_{CNP}$ (full dots) and fit (grey line) with the phenomenological relation $f(x) = sign(x)*(Ax^2+B)$ with A=0.1353$\pm$0.0003 eV V^{-2} and B=0.1675$\pm$0.0004eV, where B accounts for $E_{\rm F}$ at Vg=V$_{CNP}$[22, 23].

sample has T∼99.6-99.8%, with∼0.2-0.4% residual absorption attributed to intraband transitions enabled by disorder[72]. The T variation due to the bleaching of interband absorption is∼1.5% against the 2.3% expected for suspended SLG[8], because of the presence of the glass substrate[86].

E_F extracted from the T measurements is plotted in Fig.2c as a function of V_g. At the CNP, there is a residual p-doping E_F ∼-190meV, in agreement with the Raman estimation (∼ -230±80meV). The finite electrical conductivity and doping at the CNP[22, 23] have been attributed to the formation of electron-hole puddles[87], at the micrometer scale, that can be caused by charged impurities[88] located either in the dielectric, or at the SLG/dielectric interface[88].

We test the E_F tunability provided by the ionic liquid top-gate device up to -800meV, corresponding to a wide range of charge carrier densities from 4.5×10^{12} cm^{-2} (n-doping) to -4.7×10^{13} cm^{-2} (p-doping), much wider than possible with a standard 285nm-thick SiO_2 back gate (usually limited to∼ $\pm 6 \times 10^{12}$cm^{-2} by the gate capacitance[84]). We got similar $E_F(V_g)$ in Ref.[72] from the analysis of Raman spectra and NIR transmission.

We perform ultrafast pump-probe spectroscopy as sketched in Fig.3a. The pump is a 100fs NIR pulse centred at $\hbar\omega_{pump}$ =0.8eV, while the probe spectrum covers $\hbar\omega_{probe}$=0.729-1.240eV (see Methods for details). The relaxation dynamics is monitored through the differential transmission $\Delta T(t)/T = \frac{T_{\rm pump-ON}(t)-T_{\rm pump-OFF}}{T_{\rm pump-OFF}}$ evaluated from the probe transmission with ($T_{\rm pump-ON}$) and without ($T_{\rm pump-OFF}$) pump excitation, after a time delay t between probe and pump pulses varied with an optical delay line. Given that the pulses duration exceeds the time-scale of carrier-carrier thermalization[59], we can assume charge carriers thermalized to HFDs, and investigate their cooling dynamics.

Fig.3b plots $\Delta T/T$ at t=150fs, chosen as the delay at which the maximum signal amplitude is reached for V_g=0V. The signal is plotted as a function of E_F for different probe photon energies. Since the transient response is symmetric with respect to the CNP for n- and p- doping and our SLG is p-doped at V_g=0, we explore negative E_F in order to reach higher $|E_F|$ by applying a smaller V_g. We observe a strong modulation of $\Delta T/T$ with E_F, higher at the low energy tail of the probe pulse, with the signal changing from 4 to -2×10^{-4} (see the curve at 0.729eV in Fig. 3b). The signal amplitude decreases for increasing $\hbar\omega_{probe}$, as expected for a thermal distribution of carriers[57]. In all the probed range, near the CNP, we observe, as expected, a PB signal, *i.e.* $\Delta T/T(t) > 0$. By increasing $|E_F|$, first PB increases in amplitude, then a change of sign occurs at a threshold $|E_F|$ dependent on the probe photon energy. The Fermi energy at which the sign change occurs, $|E_F^0|$ in Fig.3c, corresponds to $\hbar\omega_{probe}/2$, *i.e.* the Pauli blocking threshold for the probe photons. Above this, the pump pulse, exciting e (h) to higher (lower) energy states, partially unblocks the probe interband absorption, otherwise inhibited, resulting in a PA signal, *i.e.* $\Delta T/T < 0$. The PA intensity increases with E_F up to a peak, whose position in terms of E_F increases with probe photon energy. A constant $\Delta T/T \sim -1 \times 10^{-5}$ is then approached in the high $|E_F|$ limit (E_F <-690meV) in all the probed range.

Above the Pauli blocking threshold for pump interband transitions ($|E_F| \geq$400meV for $\hbar\omega_{pump}$=800meV), $\Delta T/T$ is expected to vanish, because the pump should not be able to photoexcite SLG. However, a finite value is observed, caused by residual pump absorption, related to both extrinsic[16, 72, 89] and intrinsic[16, 90] effects. Amongst the former, charged impurities and scatterers (*e.g.* edge defects, cracks, vacancies) can induce residual conductivity[72, 89] activating intraband absorption. Amongst the latter, is the residual absorption from the tail of the carrier Fermi distribution, *i.e.* off-resonance absorption, which has a finite broadening at RT[90]. The fluence dependence of $\Delta T/T$ at $\hbar\omega_{probe}$ =0.729eV in the inset of Fig.3b, is superlinear above the threshold for Pauli blocking of pump absorption (as measured at $|E_F|$ =530meV), suggesting a non-negligible contribution from two-photon absorption[91]. This could also explain the vanishing signal when approaching $|E_F|$ =800meV (the Pauli blocking threshold for two-photon absorption). While height and width of PB and PA bands slightly change with $\hbar\omega_{probe}$, we observe similar features in all the probed range upon increasing $|E_F|$: an increase of PB, followed by a decrease, and a sign change above the Pauli blocking threshold for probe absorption.

To understand the E_F dependence of the non-equilibrium optical response of SLG, we calculate $\Delta T/T$ (see Methods for details) as a function of initial carrier density n_e, related to E_F by $n_e = \frac{1}{\pi}(\frac{E_F}{\hbar v_F})^2$[8], with v_F the Fermi velocity. $\Delta T/T$ in Fig.3d is computed from the changes in optical conductivity $\Delta\sigma$ induced by photoexcitation as a function of E_F. To evaluate $\Delta T/T$ at t=150fs we consider the charge carriers as distributed in energy and momentum along a HFD with a time-dependent chemical potential μ_c and $T_e(t)$ >RT. Our model takes into account that, even though the pump fluence is kept constant, the initial T_e changes with E_F due to the change of pump absorption. We consider the absorption from the finite tail of the Fermi-Dirac distribution as source of residual pump absorption for $|E_F|$ >400meV. The modification to the charge carriers distribution with E_F is sufficient to reproduce qualitatively the experimental PB signal increase, the change of sign at $\hbar\omega_{probe}/2$ and the PA decrease for E_F >400meV, Fig.3d.

To examine the dependence of the cooling dynamics on E_F, we monitor $\Delta T/T$ as a function of pump-probe delay. Figs.4a,c show the gate-dependent relaxation dynamics at $\hbar\omega_{probe}$=0.729, 1.033eV, lower and higher than

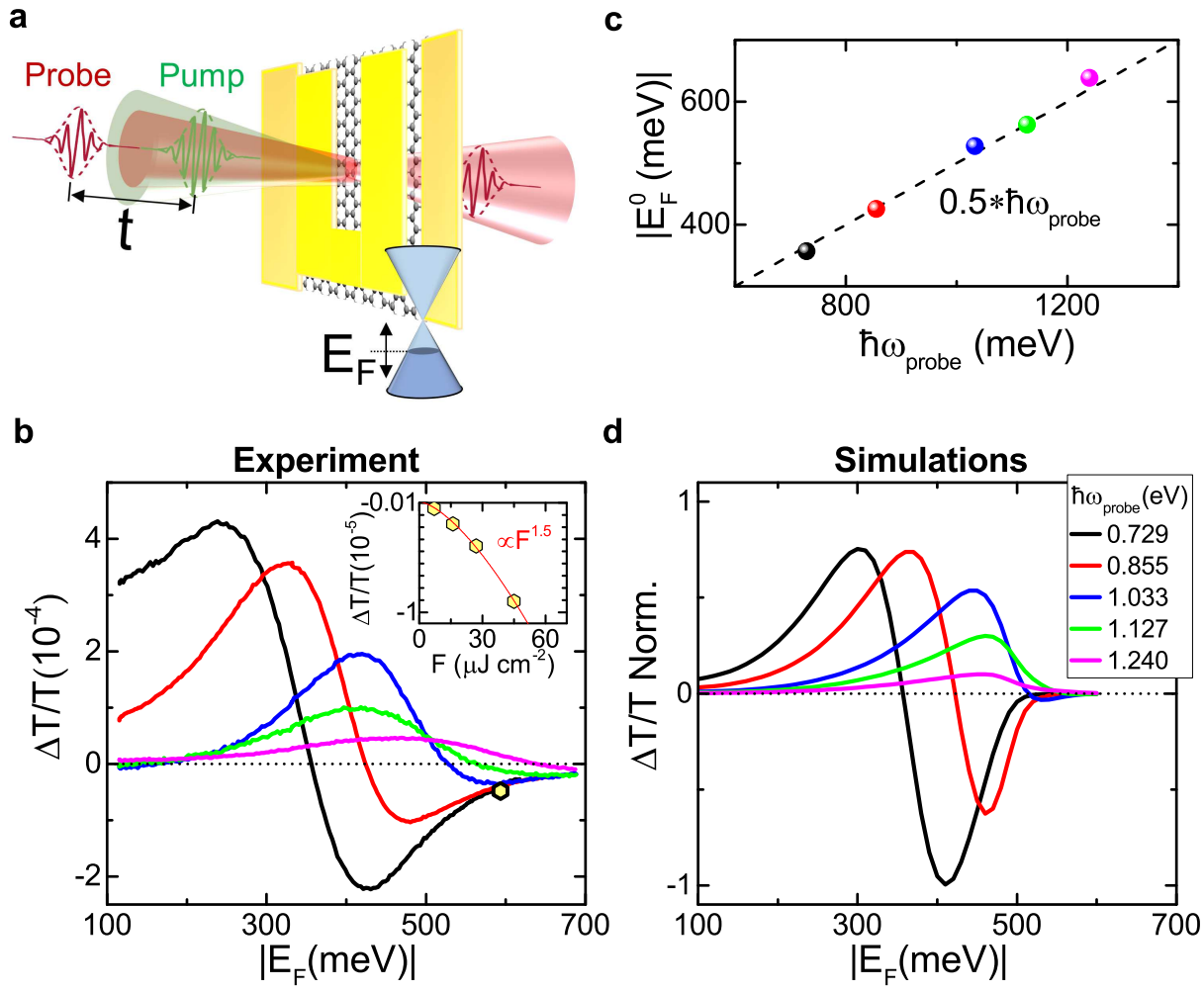

FIG. 3: (**a**) Sketch of pump-probe experiment on SLG with tunable E_F controlled by V_g. **(b)** Experimental $\Delta T/T$ at t= 150fs as a function of $|E_F|$ for p-doping acquired at different $\hbar\omega_{probe}$=0.729, 0.855, 1.033, 1.127, 1.240eV (legend of panel d) for a pump fluence F$\sim$28μJ cm^{-2}. In the inset: fluence dependence of $\Delta T/T$ absolute amplitude above Pauli blocking for pump absorption, for $\hbar\omega_{probe}$=0.729eV and E_F=0.53eV (hexagonal symbol in main figure), together with a superlinear power-law dependence on F (solid red line). **(c)** Fermi energy $|E_F^0|$ at $\Delta T/T = 0$, extracted from panel b, as a function of $\hbar\omega_{probe}$. **(d)** Simulated $\Delta T/T$ at t=150fs as a function of $|E_F|$ for p-doping at the same $\hbar\omega_{probe}$ as in panel b.

the pump photon energy. At both energies, the relaxation dynamics progressively slows down with increasing $|E_F|$, evolving from a biexponential to a monoexponential decay, due to a reduction of the fast decay component. We can appreciate this slowdown by noting that, to see a signal reduction by a factor 10, we need to wait$\sim$1ps at E_F =100meV and $\sim$5ps at 300meV. Both signal intensity and relaxation dynamics are symmetric for n- or p-doping, as a consequence of the CB,VB symmetry.

The observed gate-dependence can be qualitatively explained considering that, for increasing $|E_F|$, the excess energy of the photoexcited charge carriers with respect to equilibrium is reduced, affecting the scattering with optical phonons that drives the cooling. To gain a deeper insight into the phenomena responsible for quenching the fast relaxation component, we solve a set of phenomenological equations of motion (EOMs)[92] for the electronic temperature, T_e, and for the occupation of the phonon modes. We include the optical phonon modes at the K and Γ points of the SLG Brillouin zone, and we consider that they can be emitted/absorbed by e and h and decay into acoustic modes due to anharmonic coupling[61–63] (see Methods for details).

We calculate the time-evolution of the differential conductivity for several values of the chemical potential, μ_c, corresponding to E_F, (i.e, μ_c at T$_e$=0[90]), in the range 250 to -800meV. The results in Figs.4b,d explain the observed slowdown of the dynamics with increasing E_F with the saturation of the phase space for optical phonon-emitting electronic transitions. As E_F increases, there are fewer carriers with an energy high enough (>160meV) to emit an optical phonon, and the optical phonon emis-

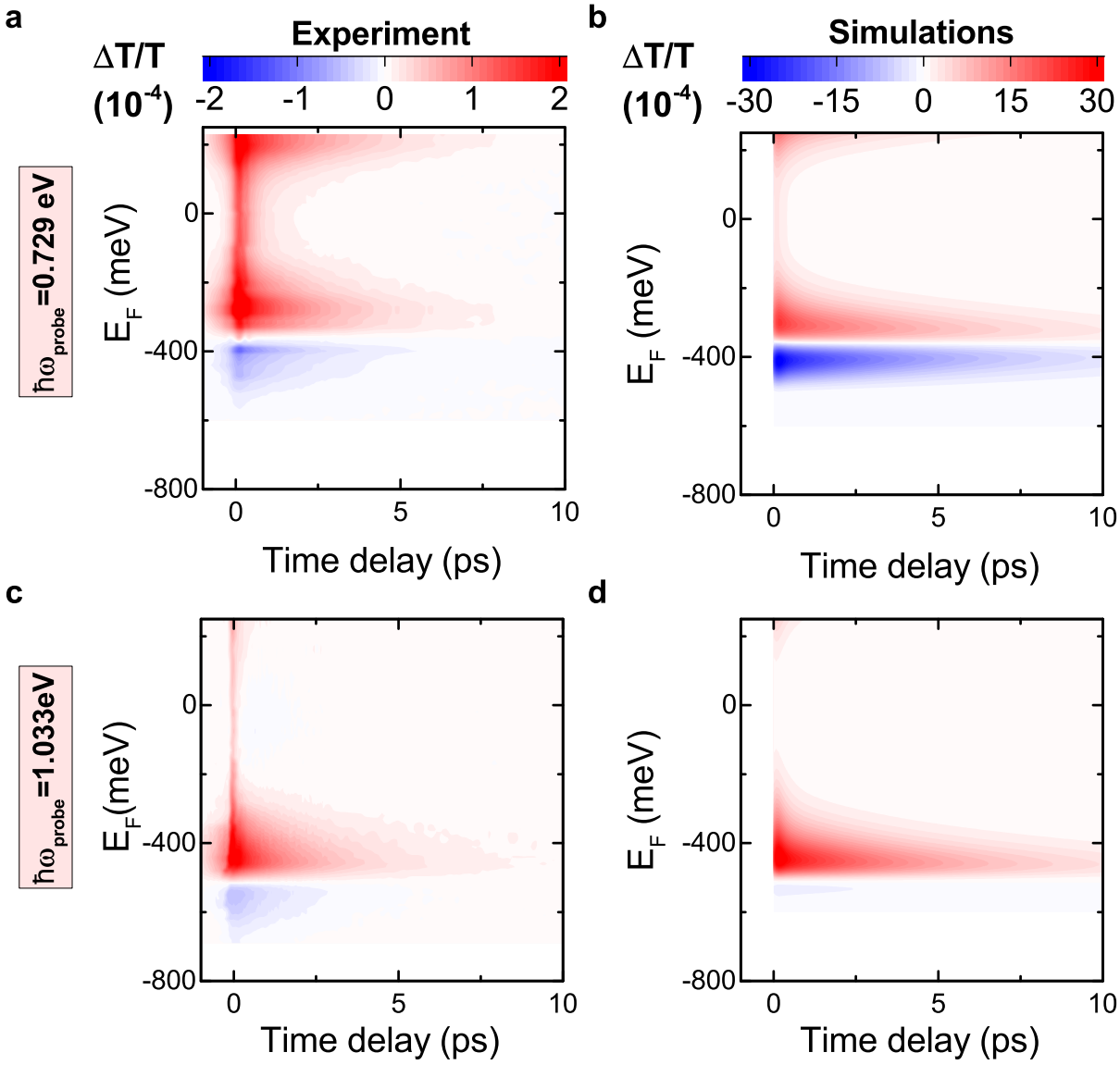

FIG. 4: Time-evolution of $\Delta T/T(t)$ for different $E_{\rm F}$ at (**a**,**b**) $\hbar\omega_{probe}$=0.729eV, with (a) Experiment, and (b) Simulations, and (**c**,**d**) $\hbar\omega_{probe}$=1.033eV, with (c) experiment and (d) simulations. $t=0$ corresponds to the pump arrival. The signal at negative delays indicates a finite build-up time, exceeding the pump-probe time duration appearing at $E_{\rm F}$=250meV for $\hbar\omega_{probe}$=0.729eV and at $E_{\rm F}$=350meV for $\hbar\omega_{probe}$=1.033eV, approaching the Pauli blocking $E_{\rm F}$

sion is quenched. This is a fundamental process, not dependent on SLG substrate, like supercollision cooling through defects[93], nor on its dielectric environment, like the cooling to hyperbolic phonons in hBN-encapsulated SLG[64]. It is determined by the intrinsic coupling of e with the K and Γ phonons[94]. The initial increase of PB amplitude with $E_{\rm F}$ in Figs.3b,c is a consequence of the quenching of relaxation *via* optical phonons[59, 62], which reduces the initial fast decay. Fig.4 also shows that the Fermi energy $|E_{\rm F}^0|$ at which the $\Delta T/T$ signal changes sign is independent of t, both in experiments and simulations. The vanishing $\Delta T/T$ does not correspond to zero absorption, but it means that the conductivity remains at its equilibrium value for all delays. For t>0, the e system is photoexcited. This can happen only because the e distribution undergoes a time-evolution such that the conductivity remains time-independent at $\hbar\omega = 2|E_{\rm F}|$.

Fig.5a shows that for $E_{\rm F}$ >340meV and $\hbar\omega_{probe}$=0.729eV, the simulations predict a further slowdown of the relaxation dynamics, not observed in our experiments. These all saturate to a similar decay trend independent on $E_{\rm F}$ (see overlapping black and green dots in Fig.5). Analogous behavior is found at all $\hbar\omega_{probe}$, provided that when we increase $\hbar\omega_{probe}$,

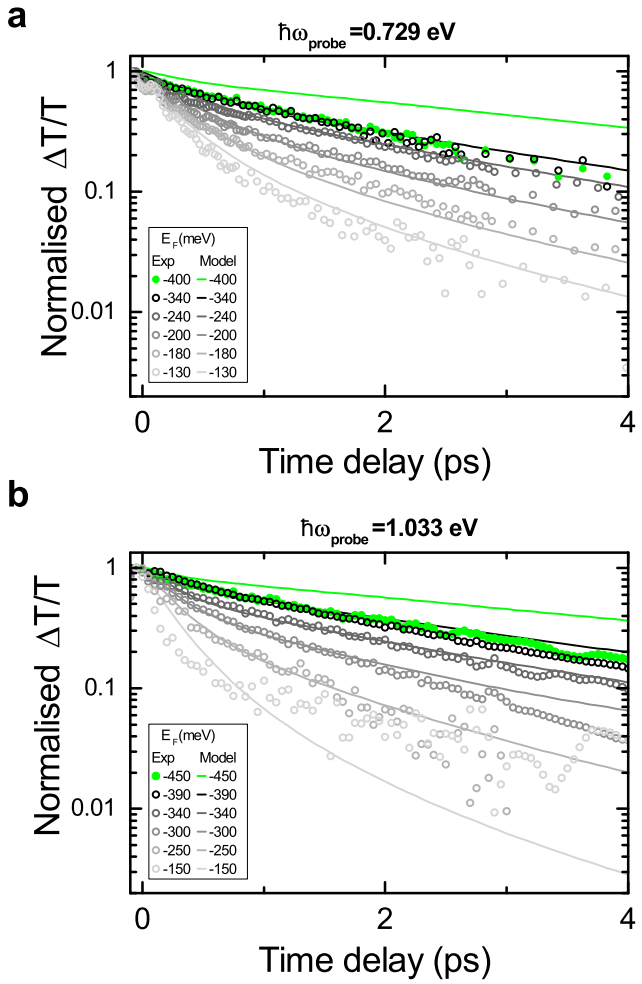

FIG. 5: (**a**-**b**) Experimental (coloured dots) and theoretical (solid lines) $\Delta T/T$ at different $E_{\rm F}$ for $\hbar\omega_{probe}$= (a) 0.729 eV and (b) 1.033eV for pump-probe time delays between -500fs and 5ps (pump arrival at t=0)

we tune E_F to higher levels to find overlapping decay dynamics(see Fig.5b). To understand the saturation of this slowdown, we need to consider that additional relaxation channels may start playing a role once the cooling *via* optical phonons gets slower. Defects can accelerate cooling[65–68], mediating the scattering with acoustic phonons of finite momentum and energy[67]. This supercollision mechanism[65–68], may become the dominating process once the optical phonon emission is quenched. Cooling times∼4ps are expected for supercollision cooling[65] in SLG with $E_{\rm F}$ ∼400meV and mobility of a few thousand cm^2 V^{-1} s^{-1}, as that of our device. The $E_{\rm F}$ independence of the decay dynamics in the high doping limit, could be explained by the lack of dependence on carrier density of the supercollision cooling time away from the Dirac point[65]. According to Refs.[77, 78], the e scattering time with defects in SLG is not expected to significantly change with $E_{\rm F}$.

The electrical tunability of the SLG relaxation dynamics, sketched in Figs.6a-c, is promising for the realization of tunable SA. Saturable absorption, *i.e.* the quenching of optical absorbance under intense illumination[95], can occur in SLG at low light intensity (*e.g.*∼0.750MW cm^{-2} at 0.8eV[96]). We measured a saturation intensity $I_{\rm S}$ = 0.5-1.7MW cm^{-2}[43] for photon energies in the range 0.5-2.5eV, comparable with that of semiconductor saturable absorber mirrors (SESAMs) (P = 0.01-0.1MW cm^{-2} at 0.944eV[97]), but maintained over a much broader spectral range[43]. The modulation depth, defined as the maximum change in absorption[95], can be optically tuned exploiting cross absorption modulation[98]. Graphene-based SAs are promising for passive mode-locking[43, 99, 100], Q-switching[101], and Q-switched mode-locking[102] of ultrafast lasers.

Fig.6 shows that the SLG equilibrium photoresponse can be electrically tuned, providing an additional knob for controlling its SA performance in terms of modulation depth and recovery dynamics, as illustrated in Fig.6. For $E_{\rm F} << \hbar\omega_{probe}/2$, the intrinsic bi-exponential-like relaxation dynamics makes SLG an ideal fast SA, Fig.6a. The presence of two different time scales, in analogy with SESAMs[103], is considered an advantage for mode locking[103]. As discussed in Refs.[103, 104], the longer time scale reduces the saturation intensity, facilitating self-starting mode-locking, while the fast relaxation component is efficient in shaping sub-ps pulses. For $E_{\rm F} \leq \hbar\omega_{probe}/2$ as in Fig.6b, SLG can act as slow SA[105] with recovery time 10 to 30 times longer than the pulse duration[105, 106], favouring soliton shaping[106], or the temporal shift of the pulses caused by the SA[103], which limits the time in which noise behind the pulse can be amplified[105]. Longer recovery time also gives an increased tolerance towards instability induced by self-phase modulation[105].

The PA at $E_{\rm F} > \hbar\omega_{probe}/2$ can be exploited to operate SLG as reverse SA[107], for which absorption increases with increasing impinging intensity, due to depletion of final state population, see Fig.6c. The PA of highly doped SLG could be exploited to realize an optical limiter[108], based on the decrease in transmittance under high-intensity or fluence illumination. An ideal optical limiter, with the functionality of protecting delicate optical elements, should strongly attenuate intense, potentially dangerous laser beams, while exhibiting high transmittance for low-intensity light. Carbon nanotubes[109] and few layer graphene[110] dispersions in organic solvents have been used to prepare optical limiters. However, these rely on nonlinear scattering[111], rather than on nonlinear absorption[112]. The nonlinear scattering of graphene dispersions[110] is based on the avalanche ionization of carbon when interacting with an incident laser pulse, and subsequent bubble formation in the solvent due to the heat released by expanding microplasmas[109, 110]. The 10ps PA lifetime of the non-

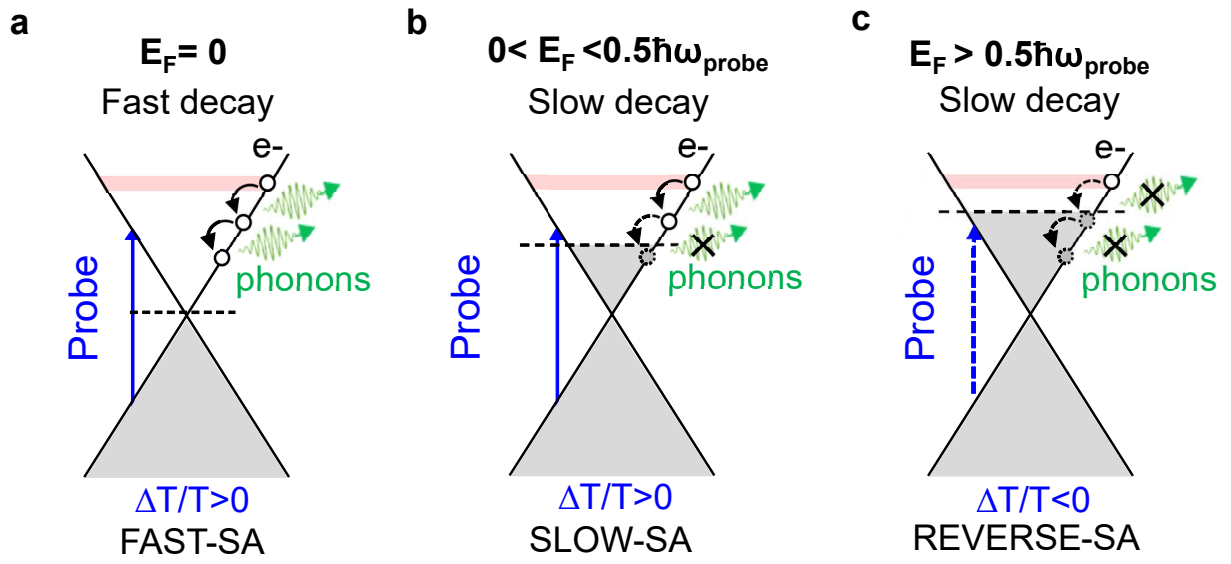

FIG. 6: (**a-c**) Sketch of interband absorption of a NIR probe pulse (vertical blue arrow) within the SLG Dirac cones populated at equilibrium up to E_F (grey filling). The pump pulse perturbs the probe absorption by promoting electrons from VB to CB (red filling), which then relax through emission of optical phonons (downward black arrows). The three sketches correspond to (a) E_F at the Dirac point, (b,c) moderate n-doping with E_F (b) below and (c) above the threshold for interband probe absorption. By increasing E_F, optical phonon emission is quenched (dashed downward arrows) and relaxation becomes slower. Above the threshold for interband absorption of the probe (dashed vertical blue arrow), the photoexcitation results in $\Delta T/T < 0$, leading to reverse saturable absorption, consisting in an increased absorption upon increasing illumination

linear absorption of highly doped SLG is 10 times shorter that the typical timescales for thermal effects and bubbling of graphene dispersions, which are of the order of 100ps[109], allowing the application to lasers with shorter pulse duration. The nonlinear absorption in SLG is not related to a specific absorption resonance of the material, thus it covers a broad spectral range (as shown in Fig.3b where for $|E_F|$=600meV we detect PA for photon energies in the range 0.729 to 1127eV). The transition from SA to reverse SA, could also be used for all-optical logic gates[113].

CONCLUSIONS

In conclusion, we demonstrated that the electrostatic tuning of the non-equilibrium optical response of SLG results in changes of amplitude, sign and recovery dynamics of $\Delta T/T$. Increasing E_F quenches emission of optical phonons, *i.e.* the fastest intrinsic relaxation channel for SLG hot charge carriers. The ability to tune E_F above the threshold for Pauli blocking of interband absorption of NIR light, results in photoinduced absorption in SLG, due to pump-induced unblocking of interband transitions for the probe. Our results pave the way to the use of voltage-controlled SLG for non-equilibrium optoelectronic devices, as a gate tunable optical element which can behave either as fast, slow, or reverse SA.

METHODS

A. High-sensitivity transient absorption microscopy

The experimental setup for the pump-probe experiments comprises a mode-locked Er-doped fiber oscillator (Toptica Photonics, FemtoFiberPro), emitting 150fs pulses at 0.8eV (1550nm) at 40MHz repetition rate. The oscillator feeds two Er-doped fiber amplifiers (EDFAs) each generating 70fs pulses at 0.8eV with 300mW average power. The output of the first EDFA is attenuated to obtain pump pulses with 1mW maximum average power. The second EDFA feeds a highly nonlinear optical fiber that produces a supercontinuum tunable between 0.73 and 1.24eV, which serves as probe pulse. The pump and probe pulses, synchronized by a computer controlled optical delay line and collinearly recombined by a dichroic beam splitter, are focused on the sample over spots of$\sim$25μm radius. The portion of the probe transmitted by the sample, spectrally selected by a monochromator with bandwidth$\sim$5nm, is detected by an amplified InGaAs photodiode (bandpass 4.5 MHz, gain 10^4) and analysed by a lock-in amplifier (Zurich Instruments HF). Pump and probe pulses have perpendicular polarizations and a linear polarizer is used to filter out the pump light scattered from the sample. The pump pulse is modulated at 1MHz by an acousto-optic modulator, resulting in a $\Delta T(t)/T$ sensitivity of the order of 10^{-7}, for an integration time of 300ms. From the FWHM of the instru-

mental response function we estimate an overall temporal resolution∼100fs. The absorbed photon density is in the range 2-3×10^{12}cm^{-2} (depending on E_F), as calculated from incident fluence and sample transmission.

B. Simulation of differential transmission dynamics

To model the time-evolution of the differential transmission, we assume that, on the time-scale given by the time-resolution of the experiment (100fs), e in both CB and VB are thermalized at the same T_e, and reach a common chemical potential $\mu_c(t)$, such that the e energy distribution is a HFD. $\mu_c(t)$ is calculated at each instant in time, as it depends on T_e, and is fixed by the condition that the carrier density, defined[90] as $n = \int_{-\infty}^{+\infty} d\varepsilon \nu(\varepsilon)[1 + exp((\varepsilon - \mu)/k_B T)]^{-1}$, with $\nu(\varepsilon)$ the electronic density of states in SLG[114], is constant[90]. As for Refs.[92, 115], we can write the following EOMs for T$_e$ and phonon occupations:

$$\begin{aligned}
\frac{dT_e(t)}{dt} &= -\frac{R_\Gamma(t)\hbar\omega_\Gamma + R_K(t)\hbar\omega_K}{c_e(t) + c_h(t)}, \\
\frac{dn_\Gamma(t)}{dt} &= \frac{R_\Gamma(t)}{M_\Gamma} - \frac{n_\Gamma(t) - n_\Gamma^{(0)}}{\tau_{ph}}, \\
\frac{dn_K(t)}{dt} &= \frac{R_K(t)}{M_K} - \frac{n_K(t) - n_K^{(0)}}{\tau_{ph}}.
\end{aligned} \tag{1}$$

Here, $n_\Gamma(t)$ and $n_K(t)$ are the occupations of the optical phonon modes at Γ and K, with energy $\hbar\omega_\Gamma \sim 0.196$eV and $\hbar\omega_K \sim 0.161$eV[94], respectively, as these have the strongest electron-phonon coupling[94]. The parameter τ_{ph} is the finite optical phonon lifetime, *via* relaxation into acoustic phonons due nonlinearities of the lattice[63], until global thermal equilibrium with densities $n_\Gamma^{(0)}$, $n_K^{(0)}$ is reached. We find good agreement between theory and experiment for $\tau_{ph} \simeq 1.2$ps, consistent with Ref.[63]. The constant coefficients M_Γ, M_K correspond to the number of phonon modes in an annular region between the minimum and maximum energy that can be exchanged with e[92, 115]. The time-dependent parameters $c_e(t)$ and $c_h(t)$ are the heat capacities of e in CB and of h in VB, respectively. The time-dependent parameters $R_\Gamma(t)$ and $R_K(t)$ are electronic relaxation rates per unit area, due to phonon emission and absorption, proportional to a Boltzmann scattering integral[92, 115].

In line with our assumption that, on the time-scale probed by our experiments, a common $\mu_c(t)$ is established between CB and VB, the heat capacities are calculated separately in the two bands, (*i.e.* T_e variations are decoupled from inter-band transitions) and only intra-band transitions are included in the relaxation rates. The initial electronic temperature $T_e(0)$, following the pump pulse, is estimated as for Ref.[37]. The initial phonon populations $n_{\Gamma,K}(0)$ are evaluated at RT. The optical photo-conductivity $\Delta\sigma(t) = \sigma(t) - \sigma(0)$[114] depends on $T_e(t)$ and $\mu_c(t)$. We use the Tinkham formula[116] to obtain the differential transmission.

[1] A. C. Ferrari *et al.*, Nanoscale **7**, 4598 (2015).
[2] F. Bonaccorso, Z. Sun, T. Hasan and A. C. Ferrari, Nat. Photonics **4**, 611 (2010).
[3] M. Romagnoli *et al.*, Nat. Rev. Mat. **3**, 392 (2018).
[4] X. Du, I. Skachko, A. Barker and E. Y. Andrei, Nat. Nanotechnol. **3**, 491 (2008).
[5] K. I. Bolotin *et al.*, Solid State Commun. **146**, 351 (2008).
[6] D. G. Purdie, N. M. Pugno, T. Taniguchi, K. Watanabe, A. C. Ferrari, A. Lombardo, Nat. Commun. **9**, 1 (2018).
[7] D. De Fazio *et al.*, ACS Nano, **13**, 8926 (2019).
[8] R. R. Nair, P. Blake, A. N. Grigorenko, K. S. Novoselov, T. J. Booth, T. Stauber, N. M. R. Peres and A. K. Geim, Science **320**, 1308 (2008).
[9] S. Pisana *et al.*, Nat. Mater. **6**, 198 (2007).
[10] A. H. Neto, F. Guinea, N. M. R. Peres, K. S. Novoselov, A. K. Geim, Rev. Mod. Phys. **81**, 109 (2009).
[11] T. Ando, Y. Zheng and H. Suzuura, J. Phys. Soc. Japan **71**, 1318 (2002).
[12] V. Gusynin, S. Sharapov and J. Carbotte, Phys. Rev. Lett. **96**, 256802 (2006).
[13] J. Horng, C. F. Chen, B. Geng, C. Girit, Y. Zhang, Z. Hao, H. A. Bechtel, M. Martin, A. Zettl, M. F. Crommie *et al.*, Phys. Rev. B **83**, 165113 (2011).
[14] F. L. Liu, Y. D. Chong, S. Adam, M. Polini, 2D Mater. **1**, 031001 (2014).
[15] O. Balci, N. Kakenov, C. Kocabas, Appl. Phys. Lett. **110**, 161102 (2017).
[16] K. F. Mak, L. Ju, F. Wang and T. F. Heinz, Solid State Commun. **152**, 1341 (2012).
[17] K. F. Mak, M. Y. Sfeir, Y. Wu, C. H. Lui, J. A. Misewich and T. H. Heinz, Phys. Rev. Lett. **101**, 196405 (2008).
[18] F. Wang, Y. Zhang, C. Tian, C. Girit, A. Zettl, M. Crommie and Y. R. Shen, Science **320**, 206 (2008).
[19] G. Liang, X. Hu, X. Yu, Y. Shen, L. H. Li, A. G. Davies, E. H. Linfield, H. K. Liang, Y. Zhang, S. F. Yu, Q. J. Wang, ACS Photonics **2**, 1559 (2015).
[20] Q. Mao, Q. Y. Wen, W. Tian, T. L. Wen, Z. Chen, Q. H. Yang, H. W. Zhang, Opt. Lett. **39**, 5649 (2014).
[21] Q. Li, Z. Tian, X. Zhang, R. Singh, L. Du, J. Gu, J. Han, W. Zhang, Nat. Commun. **6**, 7082 (2015).
[22] N. Kakenov, O. Balci, T. Takan, V. A. Ozkan, H. Altan and C. Kocabas, ACS Photonics **3**, 1531 (2016).
[23] A. Di Gaspare *et al.*, Adv. Fun. Mat., 2008039 (2020).
[24] Y. Yao, R. Shankar, M. A. Kats, Y. Song, J. Kong, M. Loncar, F. Capasso, Nano Lett. **14**, 8526 (2014).
[25] M. A. Giambra, V. Sorianello, V. Miseikis, S. Marconi, A. Montanaro, P. Galli, S. Pezzini, C. Coletti, M. Romagnoli, Opt. Express **27**, 20145 (2019).
[26] B. Zeng, Z. Huang, A. Singh, Y. Yao, A. K. Azad, A. D. Mohite, A. J. Taylor, D. R. Smith, H. T. Chen, Light Sci. Appl. **7**, 51 (2018).
[27] H. Dalir, Y. Xia, Y. Wang and X. Zhang, ACS Photonics **3**, 1564 (2016).
[28] E. O. Polat,C. Kocabas, Nano Lett. **13**, 5851 (2013).
[29] C. T. Phare, Y. D. Lee, J. Cardenas, M. Lipson, Nat.

Photonics **9**, 511 (2015).
[30] M. Liu, X. Yin, E. Ulin-Avila, B. Geng, T. Zentgraf, L. Ju, F. Wang and X. Zhang, Nature **474**, 64 (2011).
[31] V. Sorianello, M. Midrio, G. Contestabile, I. Asselberghs, J. Van Campenhout, C. Huyghebaert, I. Goykhman, A. K. Ott, A. C. Ferrari, M. Romagnoli, Nat. Photonics **12**, 40 (2018).
[32] M. Midrio, S. Boscolo, M. Moresco, M. Romagnoli, C. D. Angelis, A. Locatelli, A. D. Capobianco, Opt. Express **20**, 23144 (2012).
[33] S. Ye, Z. Wang, L. Tang, Y. Zhang, R. Lu, Y. Liu, Opt. Express **22**, 26173 (2014).
[34] J. Liu, Z. U. Khan, C. Wang, H. Zhang and S. Sarjoghian, J. Phys. D: Appl. Phys. **53**, 233002 (2020).
[35] M. Li *et al.*, Nat. Commun. **11**, 4123 (2020).
[36] A. Rahim *et al.*, Adv. Photon. **3**, 024003 (2021).
[37] G. Soavi, G. Wang, H. Rostami, D. G. Purdie, D. De Fazio, T. Ma, B. Luo, J. Wang, A. K Ott, D. Yoon *et al.*, Nat. Nanotechnol. **13**, 1 (2018).
[38] B. Buchalter and G. R. Meredith, Appl. Opt. **21**, 3221 (1982).
[39] H. G. Rosa *et al.*, Sci. Rep. **8**, 10035 (2018).
[40] N. Yoshikawa, T. Tamaya and K. Tanaka, Science **356**, 736 (2017).
[41] H. A. Hafez *et al.*, Nature **561**, 507 (2018)
[42] S. Kovalev *et al.*, Sci. Adv. **7**, eabf9809 (2021).
[43] Z. Sun, T. Hasan, F. Torrisi, D. Popa, G. Privitera, F. Wang, F. Bonaccorso, D. M. Basko and A. C. Ferrari, ACS Nano **4**, 803 (2010).
[44] S. Yu, X. Wu, K. Chen, B. Chen, X. Guo, D. Dai, L. Tong, W. Liu and Y. R. Shen, Optica **3**, 541 (2016).
[45] N. M. R. Peres, Y. V. Bludov, J.E. Santos, A. -P. Jauho and M. I. Vasilevskiy, Phys. Rev. B **90**, 125425 (2014).
[46] M. Sadeghi, V. Ahmadi, J. Opt. Soc. Am. B **35**, 528 (2018).
[47] E. Abraham, S. D. Smith, Rep. Prog. Fisica **45**, 815 (1982).
[48] T. Jiang *et al.*, Nat. Photonics **12**, 430 (2018).
[49] K. Alexander, N.A. Savostianova, S. A. Mikhailov, B. Kuyken and D. Van Thourhout, ACS Photonics **4**, 3039 (2017).
[50] A. J. Frenzel, C. H. Lui, Y. C. Shin, J. Kong, N. Gedik, Phys. Rev. Lett. **113**, 056602 (2014).
[51] S.-F. Shi, T.-T. Tang, B. Zeng, L. Ju, Q. Zhou, A. Zettl, F. Wang, Nano Lett. **14**, 1578 (2014).
[52] H. A. Hafez, P. L. Lévesque, I. Al-Naib, M. M. Dignam, X. Chai, S. Choubak, P. Desjardins, R. Martel, T. Ozaki, Appl. Phys. Lett. **107**, 251903 (2015).
[53] S. A. Mikhailov, Phys. Rev. B **100**, 115416 (2019).
[54] F. Koppens, T. Mueller, Ph. Avouris, A. C. Ferrari, M. S. Vitiello, M. Polini, Nat. Nanotech. **9**, 780 (2014).
[55] J. M. Dawlaty, S. Shivaraman, M. Chandrashekhar, F. Rana, F., and M. G. Spencer, Appl. Phys. Lett. **92**, 042116 (2008).
[56] D. Sun, Z. -K. Wu, C. Divin, X. Li, C. Berger, W. A. de Heer, P. N. First and T. B. Norris, Phys. Rev. Lett. **101**, 157402 (2008).
[57] M. Breusing, S. Kuehn, T. Winzer, E. Malić, F. Milde, N. Severin, J. Rabe, C. Ropers, A. Knorr and T. Elsaesser, Phys. Rev. B **83**, 153410 (2011).
[58] V. N. Kotov, B. Uchoa, V. M. Pereira, F. Guinea and A. C. Neto, Rev. Mod. Phys. **84**, 1067 (2012).
[59] D. Brida *et al.*, Nat. Commun. **4**, 1987 (2013).
[60] G. Cerullo, C. Manzoni, L. Lüer, D. Polli, Photochem. Photobiol. Sci. **6**, 135 (2007).
[61] M. Lazzeri, S. Piscanec, F. Mauri, A. C. Ferrari, J. Robertson, Phys. Rev. Lett. **95**, 236802 (2005).
[62] A. Tomadin, D. Brida, G. Cerullo, A. C. Ferrari and M. Polini, Phys. Rev. B **88**, 035430 (2013).
[63] N. Bonini, M. Lazzeri, N. Marzari, F. Mauri, Phys. Rev. Lett. **99**, 176802 (2007).
[64] K. -J Tielrooij *et al.*, Nat. Nanotechnol. **13**, 41 (2018).
[65] M W. Graham, S.-F. Shi, D. C. Ralph, J. Park, P. L. McEuen, Nat. Phys. **9** 103 (2013).
[66] A. C. Betz, S. H. Jhang, E. Pallecchi, R. Ferreira, G. Fève, J.-M Berroir and B. Plaçais, Nat. Phys. **9**, 109 (2013).
[67] J. C. W. Song, , M. Y. Reizer and L. S. Levitov, Phys. Rev. Lett. **109**, 106602 (2012).
[68] T. V. Alencar, M. G. Silva, L.M. Malard and A. M. de Paula, Nano Lett. **14**, 5621 (2014).
[69] I. Katayama *et al.*, Phys. Rev. B **101**, 245208 (2020).
[70] A. Das *et al.*, Nat. Nanotechnol. **3**, 210 (2008).
[71] X. Li *et al.*, Science **324**, 1312 (2009).
[72] G. Soavi *et al.*, ACS Photonics **6**, 2841 (2019).
[73] A. A. Lagatsky *et al.*, Appl. Phys. Lett. **102**, 013113 (2013).
[74] A. C. Ferrari *et al.*, Phys. Rev. Lett. **97**, 187401 (2006).
[75] A. C. Ferrari, J. Robertson, Phys. Rev. B **61**, 14095 (2000).
[76] A. C. Ferrari, D. M. Basko, Nat. Nanotechnol. **8**, 235 (2013).
[77] D. M. Basko, S. Piscanec, and A. C. Ferrari, Phys. Rev. B **80**, 165413 (2009).
[78] M. Bruna, A. K. Ott, M. Ijäs, D. Yoon, U. Sassi, and Andrea C. Ferrari, ACS Nano **8**, 7432 (2014).
[79] T. M. G. Mohiuddin *et al.*, Phys. Rev. B **79**, 205433 (2009).
[80] D. Yoon, Y.-W. Son and H. Cheong, Phys. Rev. Lett. **106**, 155502 (2011).
[81] A. Das, B. Chakraborty, S. Piscanec, S. Pisana, A. K. Sood, A. C. Ferrari, Phys. Rev. B **79**, 155417 (2009).
[82] J. Ye, S. Inoue, K. Kobayashi, Y. Kasahara, H. Yuan, H. Shimotani and Y. Iwasa, Nat. Mater. **9**, 125 (2010).
[83] H. Du, X. Lin, Z. Xu, D. Chu, J. Mater. Sci. **50**, 5641 (2015).
[84] A. K. Geim, K. S. Novoselov, Nat. Mater. **6**, 183 (2007).
[85] H. Xu, Z. Zhang, H. Xu, Z. Wang, S. Wang, and L. -M. Peng, ACS Nano **5**, 5031 (2011).
[86] C. Casiraghi, A. Hartschuh, E. Lidorikis, H. Qian, H. Harutyunyan, Hayk, T. Gokus, K. S. Novoselov and A. C. Ferrari, Nano Lett. **7**, 2711 (2007).
[87] J. Martin *et al.*, Nat. Phys. **4**, 144–8 (2008)
[88] S. Adam, E. Hwang, V. Galitski and S. D. Sarma, Proc. Natl. Acad. Sci. **104**, 18392 (2007).
[89] Z. Li, E. A. Henriksen, Z. Jiang, Z. Hao, M. C. Martin, P. Kim, H. L. Stormer and D. N. Basov, Nat. Phys. **4**, 532 (2008).
[90] C. Kittel, *Introduction to Solid State Physics* (Wiley New York, New York, 1996).
[91] A. Marini, J. D. Cox, F. J. García de Abajo, Phys. Rev. B **95**, 125408 (2017).
[92] F. Rana, P. A. George, J.H. Strait, J. Dawlaty, S. Shivaraman, M. Chandrashekhar and M. G. Spencer, Phys. Rev. B **79**, 115447 (2009).
[93] Y.-W. Song, S.-Y. Jang, W.-S. Han and M.-K. Bae, Appl. Phys. Lett. **96**, 051122 (2010).
[94] S. Piscanec *et al.*, Phys. Rev. Lett. **93**, 185503 (2004).

[95] https://www.rp-photonics.com/saturable{_}absorbers.html (accessed April 2021).
[96] F. Zhang, S. Han, Y. Liu, Z. Wang and X. Xu, Appl. Phys. Lett. **106**, 091102 (2015).
[97] G. Spühler, K. Weingarten, R. Grange, L. Krainer, M. Haiml, V. Liverini, M. Golling, S. Schön and U. Keller, Appl. Phys. B **8**1, 27 (2005).
[98] Q.-W. Sheng, M. Feng, W. Xin, H. Guo, T. -Y. Han, Y. -G Li, Y.-G. Lui, F. Gao, F. Song, Z. -B Liu *et al.*, Appl. Phys. Lett. **105**, 041901 (2014).
[99] D. Popa, Z. Sun, F. Torrisi, T. Hasan, F. Wang and A. C. Ferrari, Appl. Phys. Lett. **97**, 203106 (2010).
[100] Z. Sun, D. Popa, T. Hasan, F. Torrisi, F. Wang, E. J. Kelleher, J. C. Travers, V. Nicolosi and A.C. Ferrari, Nano Res. **3**, 653 (2010).
[101] D. Popa, Z. Sun, T. Hasan, F. Torrisi, F. Wang, A.C. Ferrari, Appl. Phys. Lett. **98**, 073106 (2011).
[102] G. Xie, J. Ma, P. Lv, W. Gao, P. Yuan, L. Qian, H. Yu, H. Zhang, J. Wang and D. Tang, Opt. Mater. Express **2**, 878 (2012).
[103] U. Keller, Nature **424**, 831 (2003).
[104] U. Keller, K. J. Weingarten, F. X. Kartner, D. Kopf, B. Braun, I. D. Jung, R. Fluck, C. Honninger, N. Matuschek and J. Aus der Au, IEEE J. Sel. Top. Quant. **2**, 435 (1996).
[105] R. Paschotta and U. Keller, Appl. Phys. B **73**, 653 (2001).
[106] F. X. Kartner, I. D. Jung, U. Keller, EEE J. Sel. Top. Quantum Electron. **2**, 540 (1996).
[107] Y.B. Band Optical Properties and Applications of Reverse Saturable Absorbers. (Springer, Boston, MA, 1986).
[108] D. J. Harter, M .L. Shand and Y. B. Band, J. Appl. Phys. **56**, 865 (1984).
[109] J. Wang and W. J. Blau, J. Phys. Chem. C **112**, 2298 (2008).
[110] J. Wang, Y. Hernandez, M. Lotya, J. Coleman and W. J. Blau, Adv. Mat. **21**, 2430 (2009).
[111] L. W. Tutt, T. F. Boggess, Prog. Quant. Elect. **17**, 299 (1993).
[112] J. Wang, W. J. Blau, J. Optics A – Pure and Appl. Optics **11**, 024001 (2009).
[113] C. Porzi, M. Guina, A. Bogoni and L. Poti, IEEE J. Sel. Top. Quant. **14**, 927 (2008).
[114] M.I. Katsnelson, *Graphene: Carbon in Two Dimensions* (Cambridge University Press, 2012).
[115] H. Wang *et al.*, Appl. Phys. Lett. **96**, 081917 (2010).
[116] M. Tinkham, Phys. Rev. **104**, 845 (1956).

ACKNOWLEDGEMENTS

This work was supported by the European Union's Horizon 2020 research and innovation programme under Grant Agreement No. 881603-GrapheneCore3. We acknowledge funding from EU Graphene Flagship, ERC Grants Hetero2D and GSYNCOR, EPSRC Grants EP/K01711X/1, EP/K017144/1, EP/N010345/1, EP/L016087/1. G.S. acknowledges the German Research Foundation DFG (CRC 1375 NOA) and the Daimler und Benz foundation.